NeuroImage: Clinical 43 (2024) 103631

Contents lists available at ScienceDirect

NeuroImage: Clinical

journal homepage: www.elsevier.com/locate/ynicl

Brain microstructure and connectivity in COVID-19 patients with olfactory or cognitive impairment

Alberto Arrigoni [a,1], Mattia Previtali [a], Sara Bosticardo [b,c,2], Giulio Pezzetti [d,3], Sofia Poloni [a,4], Serena Capelli [a,5], Angela Napolitano [d,6], Andrea Remuzzi [e,7], Rosalia Zangari [f,8], Ferdinando Luca Lorini [g,9], Maria Sessa [h,10], Alessandro Daducci [b,11], Anna Caroli [a,12,*], Simonetta Gerevini [d,13]

[a] Department of Biomedical Engineering, Istituto di Ricerche Farmacologiche Mario Negri IRCCS, Ranica, Italy
[b] Department of Computer Science, University of Verona, Italy
[c] Translational Imaging in Neurology (ThINK), Department of Biomedical Engineering, Faculty of Medicine, Basel, Switzerland
[d] Department of Neuroradiology, ASST Papa Giovanni XXIII, Bergamo, Italy
[e] Department of Management Information and Production Engineering, University of Bergamo, Dalmine, Italy
[f] FROM Research Foundation, ASST Papa Giovanni XXIII, Bergamo, Italy
[g] Department of Emergency and Critical Care Area, ASST Papa Giovanni XXIII, Bergamo, Italy
[h] Department of Neurology, ASST Papa Giovanni XXIII, Bergamo, Italy

ARTICLE INFO

Keywords:
COVID-19
Diffusion-weighted MRI
Brain Microstructure
Brain Connectivity

ABSTRACT

Introduction: The COVID-19 pandemic has affected millions worldwide, causing mortality and multi-organ morbidity. Neurological complications have been recognized. This study aimed to assess brain structural, microstructural, and connectivity alterations in patients with COVID-19-related olfactory or cognitive impairment using post-acute (time from onset: 264[208–313] days) multi-directional diffusion-weighted MRI (DW-MRI).

Abbreviations: ACC, Anterior Cingulate Cortex; ACE2, Angiotensin-Converting Enzyme 2; ALFF, Amplitude Low-Frequency Fluctuations; BBB, Blood-Brain Barrier; BCT, Brain Connectivity Toolbox; CC, Corpus Callosum; CMB, Cerebral Microbleeds; COMMIT2, Convex Optimization Modeling for Microstructure Informed Tractography 2; CSD, Constrained Spherical Deconvolution; DT, Diffusion Tensor; DW-MRI, Diffusion-Weighted MRI; FA, Fractional Anisotropy; FBA, Fixel-Based Analysis; FC, Fiber Cross-Section; FD, Fiber Density; FDC, Fiber Density and Cross-Section; FOD, Fiber Orientation Distribution; FOV, Field-Of-View; GM, Gray Matter; ICU, Intensive Care Unit; MD, Mean Diffusivity; N Acc, Nucleus Accumbens; NBS, Network-Based Statistic; OFC, Orbitofrontal Cortex; RT-PCR, Real-Time Reverse-Transcriptase Polymerase-Chain-Reaction; SyN, Symmetric Normalization; UF, Uncinate Fasciculus; WM, White Matter.

* Corresponding author at: Department of Biomedical Engineering, Istituto di Ricerche Farmacologiche Mario Negri IRCCS, Villa Camozzi via G.B. Camozzi, 3, 24020 Ranica (BG), Italy.

E-mail addresses: alberto.arrigoni@marionegri.it (A. Arrigoni), sara.bosticardo@univr.it (S. Bosticardo), gpezzetti@asst-pg23.it (G. Pezzetti), sofia.poloni@marionegri.it (S. Poloni), serena.capelli@marionegri.it (S. Capelli), anapolitano@asst-pg23.it (A. Napolitano), andrea.remuzzi@unibg.it (A. Remuzzi), rzangari@fondazionefrom.it (R. Zangari), llorini@asst-pg23.it (F.L. Lorini), msessa@asst-pg23.it (M. Sessa), alessandro.daducci@univr.it (A. Daducci), anna.caroli@marionegri.it (A. Caroli), sgerevini@asst-pg23.it (S. Gerevini).

[1] orcid.org/0000-0002-1914-6582.
[2] orcid.org/0000-0002-0063-2521.
[3] orcid.org/0009-0006-6057-9685.
[4] orcid.org/0000-0002-9402-9925.
[5] orcid.org/0000-0002-8450-3806.
[6] orcid.org/0000-0001-8423-4485.
[7] orcid.org/0000-0002-4301-8927.
[8] orcid.org/0000-0002-4425-7866.
[9] orcid.org/0000-0002-2711-3377.
[10] orcid.org/0000-0002-9589-0290.
[11] orcid.org/0000-0002-4677-6678.
[12] orcid.org/0000-0002-4130-4663.
[13] orcid.org/0000-0002-2374-194X.

https://doi.org/10.1016/j.nicl.2024.103631
Received 5 March 2024; Received in revised form 31 May 2024; Accepted 11 June 2024
Available online 12 June 2024

Neuroinflammation
Neurodegeneration

Methods: The study included 16 COVID-19 patients with cognitive impairment (COVID-CM), 35 COVID-19 patients with olfactory disorder (COVID-OD), and 14 controls. A state-of-the-art processing pipeline was developed for DW-MRI pre-processing, mean diffusivity and fractional anisotropy computation, fiber density and cross-section analysis, and tractography of white-matter bundles. Brain parcellation required for probing network connectivity, region-specific microstructure and volume, and cortical thickness was based on T1-weighted scans and anatomical atlases.

Results: Compared to controls, COVID-CM patients showed overall gray matter atrophy (age and sex corrected $p = 0.004$), and both COVID-19 patient groups showed regional atrophy and cortical thinning. Both groups presented an increase in gray matter mean diffusivity (corrected $p = 0.001$), decrease in white matter fiber density and cross-section **(corrected $p < 0.05$)**, , and COVID-CM patients also displayed an overall increased diffusivity ($p = 0.022$) and decreased anisotropy (corrected $p = 0.038$) in white matter. Graph-based analysis revealed reduced network modularity, with an extensive pattern of connectivity increase, in conjunction with a localized reduction in a few connections, mainly located in the left hemisphere. The left cingulate, anterior cingulate, and insula were primarily involved.

Conclusion: Expanding upon previous findings, this study further investigated significant alterations in brain morphology, microstructure, and connectivity in COVID-19 patients with olfactory or cognitive disfunction. These findings suggest underlying neurodegeneration, neuroinflammation, and concomitant compensatory mechanisms. Future longitudinal studies are required to monitor the alterations over time and assess their transient or permanent nature.

1. Introduction

The COVID-19 pandemic resulted in worldwide mortality and morbidity primarily attributed to respiratory complications. However, the scientific community has increasingly recognized that the disease and its long-term sequelae, referred to as Long COVID chronic illness, extend beyond respiratory consequences. In particular, studies documented approximately 200 diverse clinical manifestations across 10 organ systems (Davis et al., 2021), including olfaction and cognitive disorders (Guo et al., 2022).

Cognitive deficits account for brain fog, word-finding problems, and impairments in attention, executive function, decision-making, problem-solving, and memory consolidation (Davis et al., 2021; Guo et al., 2022). Mechanisms underlying these neurological disorders are likely associated with direct viral invasion, neuroinflammation, hypoxia, cerebral vascular events, and dysregulated immune responses (Lou et al., 2021).

Olfactory total or partial impairment (anosmia and hyposmia) has emerged as a prominent clinical feature of COVID-19. Olfaction significantly impacts an individual's well-being and leverages their behaviour, personality, and social interactions(Sarafoleanu et al., 2009); its disruption typically appears early in the disease course and persists, affecting around 40 % of patients (Guo et al., 2022; Karamali et al., 2022; Lechien et al., 2023). Studies suggest that COVID-19-related smell dysfunction is not associated with nasal obstruction and rhinitis but might result from COVID-19 neurovirulence and the infection of the olfactory mucosa. Supporting this hypothesis, a previous study we conducted revealed damage and atrophy in the olfactory bulbs of COVID-19 patients with neurological symptoms (Capelli et al., 2023).

Diffusion-weighted magnetic resonance imaging (DW-MRI) is an advanced MRI technique that enables probing brain microarchitecture integrity and inferring the shape and organization of white matter tracts through tractography. The latter allows for assessing brain connectivity, providing insight into pathological mechanisms such as demyelination, edema, neuroinflammation, and axonal degeneration (Assaf and Pasternak, 2008).

Brain connectivity analysis exploits graph theory, which provides a mathematical framework to characterize the brain as a network of nodes (gray matter regions) connected by edges (white matter fiber tracts) and compute various graph measures probing the topological properties of the brain network (Rubinov and Sporns, 2010).

Recent studies investigating brain-related abnormalities in COVID-19 patients revealed involvement of the left-brain hemisphere and a reduction in grey matter thickness, particularly in the parahippocampal gyrus, anterior cingulate cortex (ACC), temporal pole, left orbitofrontal cortex (OFC), insula, and supramarginal gyrus. Mean diffusivity increase was also reported, mainly in the OFC, ACC, left insula, and amygdala, (Douaud et al., 2022) and hypometabolism was observed in a network of functionally related areas encompassing the prefrontal cortex, ACC, insula, and caudate nucleus in patients with acute COVID-19-related encephalopathy (Kas et al., 2021).

To date, COVID-19-related studies investigating brain structural connectivity are still few, with Esposito et al. and Bispo et al. focusing on olfactory-related areas in patients with persisting hyposmia (Bispo et al., 2023; Esposito et al., 2022) and Tassignon et al. comparing cognitive performance in non-intensive care unit (ICU)- and ICU-treated survivors (Tassignon et al., 2023).

Our study aimed to use state-of-the-art DW-MRI processing techniques to provide insight into brain structure, microstructure and connectivity alterations associated with olfactory or cognitive deficits following SARS-CoV-2 infection, thus improving the clinical management of COVID-19 patients with neurological complications.

2. Materials and methods

2.1. Study design and patient selection

Confirmed COVID-19 patients who underwent brain MRI examination, including T1-weighted and DW-MRI scans, due to COVID-19-related neurological complications were eligible for inclusion. We considered patients who revealed predominant cognitive symptoms (COVID-CM) in the anamnesis interview, including memory deficits (14/16), insomnia (1/16), confusion (2/16), and attention impairment (1/16), and patients with olfactory dysfunction (COVID-OD), characterized by at least partial anosmia and the absence of other severe neurological signs. Within the COVID-OD group, 19 out of 35 patients experienced concurrent partial or total ageusia, while among the 16 COVID-CM patients, anosmia and ageusia were concomitantly present in 7 patients. No patients reported parosmia. The frequency of individual neurological symptoms reported by COVID-OD and COVID-CM patients are displayed in Table 1. Patients with pre-existing neurological disorders or brain parenchymal lesions were excluded from the study. Patients showing COVID-19-related cerebrovascular disorders with parenchymal lesions were further excluded. Patients who underwent brain T1-weighted and DW-MRI for reasons other than COVID-19 and were negative to MRI findings were included in the study as control patients (CTRL) if they didn't show any clinical history of COVID-19 disease or related symptoms and resulted negative when testing for the disease at the time of the MRI. Cases with inappropriate field-of-view extension (FOV), morphological alteration possibly affecting the image

Table 1
Neurological symptoms reported by COVID-19 patients with cognitive deficit (COVID-CM, n = 16) or olfactory disorder (COVID-OD, n = 35) included in the study.

Group	Reported Neurological Symptom	Parcellation Node
CM	memory deficits	14/16
	insomnia	1/16
	confusion	2/16
	attention impairment	1/16
	anosmia	7/16
	ageusia	7/16
OD	memory deficits	0/35
	insomnia	0/35
	confusion	0/35
	attention impairment	0/35
	anosmia	35/35
	ageusia	19/35

processing (e.g., enlarged ventricles), and technical processing failures were excluded.

The local ethics committee approved collecting and using patients' data for research purposes within the framework of a broader observational study protocol (Reg. 118/22). Informed consent was obtained from patients or their next of kin.

2.2. COVID-19 diagnosis

The COVID-19 diagnosis was confirmed by real-time reverse-transcriptase polymerase-chain-reaction (RT-PCR) on at least one nasopharyngeal swab; RT-PCR on bronchoalveolar lavage when suspected SARS-CoV-2 infection despite negative results from at least two nasopharyngeal swabs 24 h distant; or typical clinical presentation (fever, dry cough, and dyspnea) and radiological evidence of interstitial pneumonia when negative RT-PCR.

2.3. MRI acquisition

Brain MRI scans were acquired between June 2020 and October 2021 in the Neuroradiology Unit of the ASST Papa Giovanni XXIII hospital in Bergamo, Italy, with a General Electric 3 T MRI scanner (GE Discovery MR750w; GE Healthcare, Chicago, Illinois).

In case of COVID-19 patients, the MRI acquisition protocol included a DW-MRI single-shell scan (TR: 14000 ms; TE: 84 ms; b-values: 0 and 1000; number of directions: 32; voxel size: 1x1x2 mm; matrix size: 256x256x57; phase encoding: PA) and a T1-weighted axial scan (TR: 600 ms; TE: 9 ms; voxel size: 0.5x0.5x3 mm, slice gap: 0.4 mm; matrix size: 512x512x40).

In the case of control patients, the MRI acquisition protocol included the two sequences with slightly different acquisition parameters. Specifically, the DW-MRI scans were acquired with voxel size 1x1x3 mm and matrix size 256x256x45, and the T1-weighted axial scan with TR and TE equal to 7 and 3 ms, respectively, voxel size 0.45x0.45x3 mm, no slice gap, and matrix size 512x512x48.

2.4. MRI processing

An in-house MRI processing pipeline was developed in MATLAB (vR2021a, https://www.mathworks.com/) and Python (v3.7.10; https://www.python.org/), using the following tools: MRtrix3Tissue (v5.2.9; https://3Tissue.github.io), MRtrix3 (v3.0.4; https://www.mrtrix.org/), FSL (v6.0.5; https://fsl.fmrib.ox.ac.uk/fsl/fslwiki/), SPM12 (v7771; https://www.fil.ion.ucl.ac.uk/spm/), FreeSurfer (v7.3.0; https

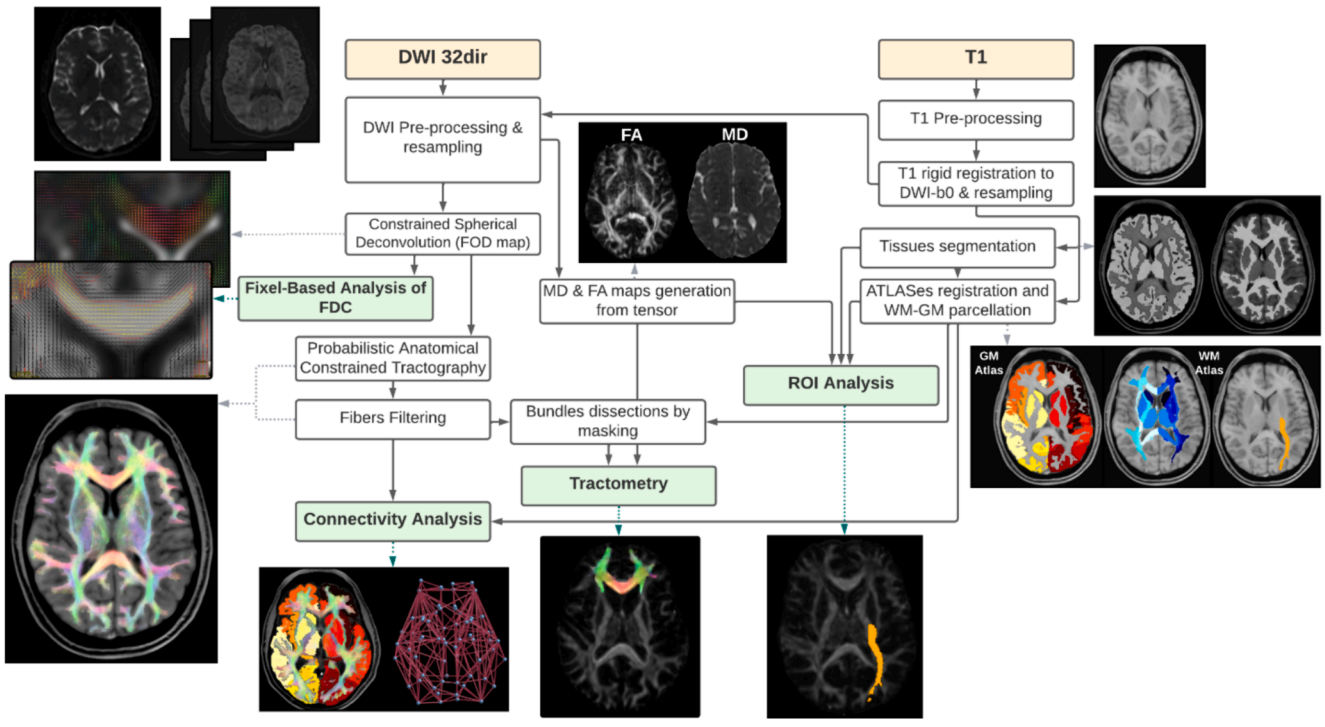

Fig. 1. Schematic representation of the MRI processing pipeline. Both the T1-weighted and the 32-direction diffusion-weighted MRI (DW-MRI) scans first undergo pre-processing to correct for possible noise, artifacts, and distortions. The DW-MRI scan is then processed to derive the tensor image with the pertinent Mean Diffusivity (MD) and Fractional Anisotropy (FA) maps. Constrained spherical deconvolution is applied to estimate the Fiber-orientation Distribution Image (FOD), subsequently normalized. A probabilistic algorithm generates the streamlines' tractography from the FOD, and the reconstructed fibers are filtered using a model that best fits the diffusion signal. FOD images are also used as the basis for the fixel-based analysis of the Fiber Density and Cross-section (FDC). The pre-processed T1 scan, after registration to the DWI-b0 scan, undergoes gray matter (GM) and white matter (WM) segmentation and is then used in combination with GM and WM anatomical atlases to parcellate the brain into tissues and regions. DW-MRI and T1 processing outputs are finally combined to investigate connectivity and microstructure, with the latter examined by both ROI analysis and tractometry.

://surfer.nmr.mgh.harvard.edu), and ANTs (v2.3.5; https://stnava.github.io/ANTs/). The pipeline included several steps: correction of noise, artifacts, and distortions in the input scans; regional parcellation using the T1-weighted scan and anatomical atlases; and estimation of diffusion indices, CSD, fixel-based analysis, tractography, and connectomics on the DW-MRI scan (Fig. 1).

2.5. T1-weighted MRI processing

T1-weighted scans were intensity normalized using FreeSurfer. The T1-weighted scans and FreeSurfer resulting segmentation ("aseg" file) were then co-registered to the space of DW-MRI images using ANTs. Subsequently, the brain regions and tissues, particularly white matter (WM) and gray matter (GM), were also segmented with SPM12 to improve the overall accuracy. The T1-weighted pre-processed images also served as a reference for non-linear Symmetric Normalization (SyN) of anatomical atlases using ANTs. The non-linear transformation, optimized for mutual information, was applied to the atlases labelling GM regions and WM tracts and bundles to warp and fit them to the patient-specific morphology.

The brain parcellation included 65 GM regions identified by grouping 170 detailed regions from the AAL3 atlas (https://www.gin.cnrs.fr/en/tools/aal/), 42 WM bundles from the IIT atlas (https://www.nitrc.org/projects/iit/), and 118 WM regions from the JHU Type III atlas (https://github.com/Jfortin1/EveTemplate). The latter was reduced to 102 WM regions by imposing a dimensionality threshold of 150 voxels to avoid considering regions too small to ensure a reliable analysis. Specifically, the superficial WM angular, pre-cuneus, cuneus, lingual, fusiform, entorhinal, rectus and amygdala regions, as well as the uncinate fasciculus and fornix were excluded. All regions were masked with the pertinent patient-specific tissue segmentation.

FreeSurfer also allowed estimating the brain segmentation volume excluding the brainstem (BrainSegVol) and computing the average thickness in the Desikan-Killany cortical surface partition.

2.6. DW-MRI pre-processing

DW-MRI scans were pre-processed using MRtrix3Tissue functions, including denoising, Gibbs ringing artifact removal, and correction of Eddy-current-induced distortions. The SPM12-based cerebrospinal fluid (CSF) segmentations obtained on the DW-MRI-b0 and T1-weighted scans were co-registered using SyN to estimate susceptibility-induced distortion since no reverse phase-encoding scan was available. The resulting transformation was applied to the whole DW-MRI scans while preserving each subject's native space. Bias field correction was lastly performed. The corrected DW-MRI scans were up-sampled to a 1x1x1 isotropic voxel size to improve tractography results. The diffusion gradient scheme was updated during pre-processing.

2.7. Diffusion tensor and volumetric analysis

The pre-processed DW-MRI scans were used to estimate the diffusion tensor (DT).

The DT provides insights into the magnitude and directionality of water molecules' diffusion in tissues via quantitative metrics such as Fractional Anisotropy (FA) and Mean Diffusivity (MD). FA represents the degree of directional coherence of water diffusion within a voxel; MD quantifies the average magnitude of water diffusion and is sensitive to tissue density and microstructure changes.

A custom MATLAB script was developed to assess diffusion indices in individual brain tissues and regions by masking the FA and MD maps with the pertinent segmentations and computing the median statistics.

Individual brain tissue and region volumes were also assessed by counting the number of voxels within each region of interest and multiplying this count by the dimensions of the voxels. Volumes were normalised to the patient-specific BainSegVol, retrieved from FreeSurfer stats report.

2.8. Tractography

Despite allowing the inference of the shape and organization of white matter tracts, the DT has limitations in resolving complex fiber configurations, such as crossing bundles. The Constrained Spherical Deconvolution (CSD) addresses this limitation, mapping the complex connectivity patterns of the brain (Tournier et al., 2004).

In particular, the "dhollander" algorithm was employed to compute a unique average set of WM, GM, and CSF response functions from a subset of 8 COVID-19 and 8 age- and sex-matched control patients, enabling the Single-Shell 3-Tissue CSD to obtain the tissue-specific Fiber Orientation Distribution (FOD) images, subsequently normalized via multi-tissue informed log-domain intensity normalisation. Then, the whole-brain tractography was performed using the iFOD2 probabilistic algorithm to generate 3 million streamlines, as suggested by (Gabusi et al., 2024), exploiting the brain tissue segmentation in the five-tissue-type (5TT) format computed with FreeSurfer as anatomical constraint. Finally, the tractogram was processed with Convex Optimization Modeling for Microstructure Informed Tractography 2 (COMMIT2), using the "Ball&Sticks" forward model to filter false positive connections as well as to obtain biologically accurate estimates of the brain's structural connectivity (Schiavi et al., 2020).

2.9. Tractometry

WM bundle segmentations were also used as a mask to edit the tractogram, isolating streamlines within their respective bundle regions. Tractometry analysis was then conducted on the dissected tractography bundles by sampling median values of FA and MD along the tracks. To derive an aggregate measure indicative of the overall microstructural integrity of each bundle, we computed the median value of FA and MD across the fiber-wise statistics.

2.10. Fixel-based analysis

Fixel-based analysis (FBA) was additionally carried out, following a state-of-the-art protocol (Dhollander et al., 2021), to probe further microstructure and leverage CSD potential in dealing with complex fiber configurations. FBA allowed assessment of Fiber Density (FD), representing the number of fibers packed into a single voxel, and Fiber Cross-Section (FC), which indicates the proportion of the voxel occupied by the fiber bundle. Local reductions in patients compared to controls in FD, FC and the combined measure of Fiber Density and Cross-Section (FDC) were investigated.

Group-specific FOD templates were generated for COVID-CM and COVID-OD patients, separately, using a subset of 14 FOD images from patients and 14 FOD images from control subjects. Subsequently, individual FOD images were registered to their corresponding template. This warp transformation was also applied to subject-specific DW-MRI-derived brain masks. Masks from all subjects were intersected to obtain a unique common-voxels mask to restrict the analysis to voxels common to all subjects.

Fixels and FD were then estimated from the FOD images. Fixels reorientation was performed to ensure their directions were consistent with the brain anatomy in transformed FOD images. Subject fixels were subsequently assigned to template fixels to locate FD values in the template space. Additionally, the log scaled FC metric was computed based on the warp from FOD registration. FDC was finally computed by combining FD and FC.

Fixel-based analysis employed connectivity-based fixel enhancement. In this stage, a new whole-brain fiber tractography was performed on the FOD template, generating 20 million streamlines, followed by SIFT filtering, ultimately resulting in a new whole-brain tractogram with 2 million streamlines.

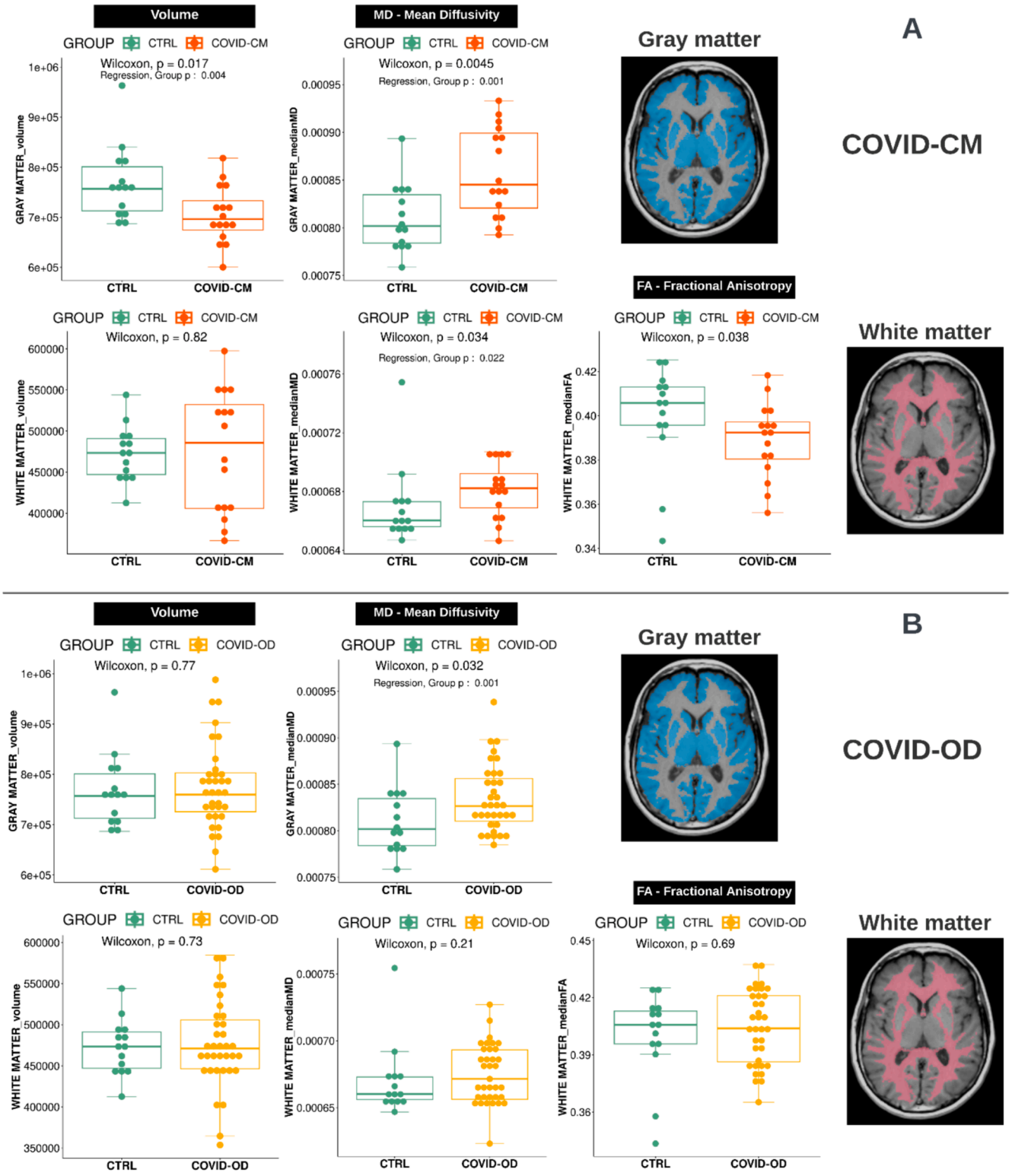

Fig. 2. Volume (left column), Fractional Anisotropy (FA, middle column), and Mean Diffusivity (MD, right column) distributions in the white and gray matter in COVID-19 patients with cognitive deficit (COVID-CM, n = 16; panel A, top rows, in orange) or olfactory disorder (COVID-OD, n = 35; panel B, bottom rows, in yellow) as compared with normal controls (CTRL, n = 14; green boxplots). P-values were computed using the Wilcoxon-Mann-Whitney test. T-test p-values of the group variable in the regression model accounting also for sex, age, and brain volume of the subjects are reported when significant ($p < 0.05$). The examples of the segmented tissue on the right are taken from a representative COVID-19 patient, specifically a 54-year-old female.

2.11. Connectivity analysis

The resulting tractogram was combined with the GM parcellation to compute the connectomes and thus perform graph-based analysis. Structural connectivity was assessed using the Brain Connectivity Toolbox (BCT; https://sites.google.com/site/bctnet/) by selecting specific global measures related to the overall network, and local measures related to individual nodes. In particular, we considered: *modularity*,

Table 2
Fractional Anisotropy (FA) and Mean Diffusivity (MD) in individual gray and white matter regions in COVID-19 patients with cognitive and memory deficit (COVID-CM, n = 16) or olfactory disorder (COVID-OD, n = 35) as compared with normal controls (CTRL, n = 14). The distribution of the most significant differences ($p \leq 0.001$) is displayed as median [IQR], and the MD values (mm^2/s) were multiplied by 10^3. P-values were computed by *t*-test in a multiple linear regression estimated with a robust model also considering the age and sex of the subjects. Reported differences stay significant (p adjusted < 0.050) after correcting for multiple comparisons via the Holm–Bonferroni method, accounting for 65 comparisons for gray matter and 102 for white matter. Abbreviations: ACC: anterior cingulate cortex; C: cingulum; CC: corpus callosum; F: fornix; OFC: orbitofrontal cortex; OPT: occipitopontine tract; PPT: parietopontine tract; UF: uncinate fasciculus.

Tissue	Diffusion parameter	Parcellation Node	COVID-CM	CTRL	p	Direction
GM	MD	Frontal R	0.98[0.92–1.02]	0.85[0.82–0.87]	**<0.001**	↑
		Frontal L	0.97[0.90–1.01]	0.83[0.81–0.87]	**<0.001**	↑
		Parietal L	1.11[1.03–1.19]	0.95[0.89–1.01]	**<0.001**	↑
		Precentral R	0.91[0.87–1.00]	0.82[0.78–0.83]	**<0.001**	↑
		Parietal R	1.16[1.05–1.27]	0.97[0.91–1.02]	**0.001**	↑
WM	FA	Medulla L	0.22[0.12–0.26]	0.45[0.43–0.48]	**<0.001**	↓
		Medulla R	0.30[0.25–0.32]	0.46[0.42–0.48]	**<0.001**	↓
	MD	Medulla R	0.94[0.82–1.42]	0.68[0.67–0.70]	**<0.001**	↑
		CC ForcepsMinor Bundle	0.73[0.73–0.74]	0.71[0.69–0.72]	**<0.001**	↑
		Medulla L	1.68[1.15–2.25]	0.70[0.66–0.74]	**<0.001**	↑
		Inferior cerebellar peduncle R	0.65[0.64–0.67]	0.61[0.61–0.62]	**<0.001**	↑
		Posterior corona radiata R	0.72[0.69–0.74]	0.68[0.65–0.69]	**<0.001**	↑
		Middle cerebellar peduncle R	0.60[0.60–0.61]	0.59[0.57–0.59]	**<0.001**	↑
Tissue	**Diffusion parameter**	**Parcellation Node**	**COVID-OD**	**CTRL**	**p**	**Direction**
GM	MD	Frontal L	0.92[0.88–0.96]	0.83[0.81–0.87]	**<0.001**	↑
		Frontal R	0.93[0.88–0.97]	0.85[0.82–0.87]	**<0.001**	↑
		Parietal L	1.02[0.94–1.09]	0.95[0.89–1.01]	**<0.001**	↑
		Precentral L	0.89[0.85–0.95]	0.83[0.81–0.86]	**<0.001**	↑
		Cuneus R	0.93[0.89–1.02]	0.84[0.82–0.90]	**<0.001**	↑
		Parietal R	1.03[0.96–1.11]	0.97[0.91–1.02]	**<0.001**	↑
		Precentral R	0.88[0.84–0.92]	0.82[0.78–0.83]	**0.001**	↑
WM	FA	Medulla L	0.26[0.21–0.32]	0.45[0.43–0.48]	**<0.001**	↓
		Medulla R	0.34[0.25–0.39]	0.46[0.42–0.48]	**<0.001**	↓
		Middle cerebellar peduncle R	0.50[0.48–0.52]	0.54[0.53–0.57]	**<0.001**	↓
	MD	Inferior cerebellar peduncle R	0.66[0.65–0.67]	0.61[0.61–0.62]	**<0.001**	↑
		Middle cerebellar peduncle R	0.61[0.60–0.62]	0.59[0.57–0.59]	**<0.001**	↑

computed via the Louvain algorithm, which informs on the extent to which the network can be divided into modules; global and local *efficiency*, representing the inverse of the average of the shortest path length across all network's nodes and, locally, between a node and its neighbours; *density*, measuring the fraction of existing connections to possible ones; *clustering coefficients*, indicating the fraction of triangles around a node; and *degree* and *strength*, informing on the sums of each node's connections and their structural weights, respectively (Rubinov and Sporns, 2010).

Despite patients' exclusion from the study due to major FOV cuts, specific apical and basal brain regions were discarded from the connectivity assessment to account for minor residual differences in the FOV's fitting. Specifically, the brain network excluded the cerebellum, vermis, supplementary motor areas, and paracentral lobules in both patients and controls.

Connectivity analysis was initially performed on the overall brain network and, subsequently, on the emerging altered subnetworks, also probed by tractometry.

2.12. Statistical analysis

Statistical analysis was performed using R software (v4.3.0; https://www.r-project.org/), MATLAB, and Python. Continuous variables were described as median [IQR]. The Wilcoxon-Mann-Whitney test was initially used to identify significant differences between COVID-19 groups and control patients, setting the statistical significance threshold at $p < 0.05$.

In the subset of measures showing significant differences, regression analysis was performed to account for sex and age differences. In this case, the statistical significance threshold was set at $p < 0.01$. Whole-brain measures were also corrected for patient-specific BrainSegVol, setting the statistical significance threshold at $p < 0.05$. In cases of multiple comparisons, p-values were corrected using the Holm-Bonferroni method (adjusted $p < 0.05$).

In the connectivity analysis, the median connectomes, describing the distribution of the structural connection weights in patient groups and controls, were also computed; significant differences in individual connections were assessed using mass-univariate testing by the Wilcoxon-Mann-Whitney test ($p < 0.01$).

The MATLAB Network-Based Statistic (NBS) tool (v1.2; https://www.nitrc.org/projects/nbs/) was finally used to extract impaired or increased connectivity subnetworks. This tool allowed for T-test while correcting for multiple comparisons through a nonparametric statistical method (Zalesky et al., 2010), also called NBS (T-test threshold: 3.1; $p < 0.05$; permutations: 15000), taking age and sex into account.

FDC statistical analysis employed connectivity-based fixel enhancement, a general linear model and non-parametric permutation testing to correct for multiple comparisons. Sex and age were set as covariates in the general linear model.

3. Results

3.1. Patient population

Among the eligible 94 COVID-19 patients, 21 exhibited cognitive deficits as the predominant COVID-19-related neurological consequence (COVID-CM group), and 47 had olfactory dysfunction only (COVID-OD group). A total of 17 patients, 12 from the COVID-OD group and 5 from the COVID-CM group, were not considered due to exclusion criteria. In detail, 2 and 5 patients were excluded from the COVID-CM and COVID-OD groups due to FOV inadequacies, 2 and 1 due to enlarged ventricles, and 1 and 6 due to technical failure, respectively.

The final study population comprised 16 COVID-CM and 35 COVID-OD patients, as shown in the study flowchart (Supplementary Fig. 1). The CTRL group included 14 individuals with similar age to the COVID-CM patients (CTRL: 62[45–70] years old; COVID-CM: 56[51–61] years old; Wilcoxon-Mann-Whitney $p = 0.54$). On the contrary, COVID-OD patients were younger than controls (COVID-OD: 40[31–53] years;

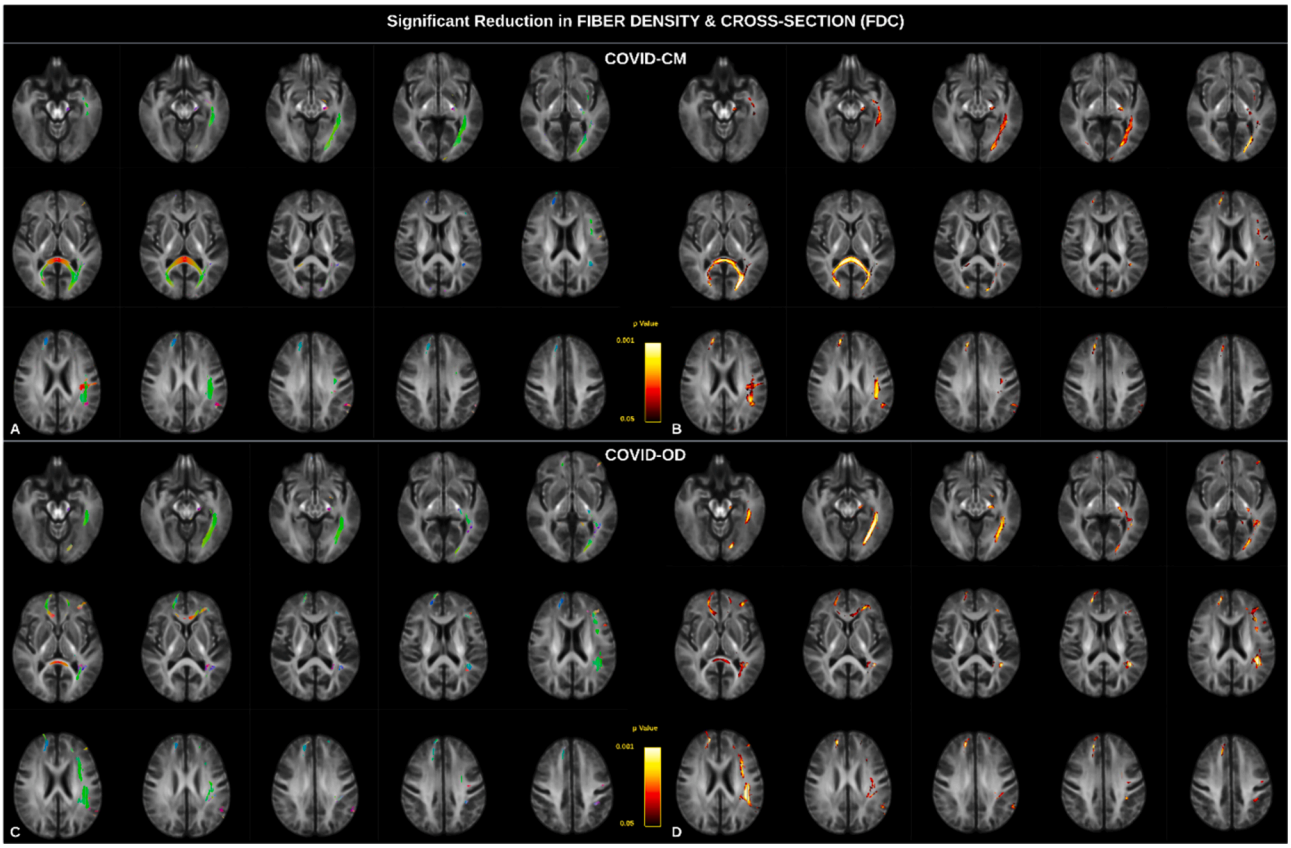

Fig. 3. Fiber Density and Cross-Section (FDC) alterations in COVID-19 patients with cognitive deficit (COVID-CM, panels A and B, top row) or olfactory disorder (COVID-OD, panels C and D, bottom row) as compared with normal controls. All four panels show fixels with significant reduced FDC in patients ($p < 0.05$). In the left column (panels A and C), the color represents altered fixels orientation, and in the right column, the color scale represents statistical significance. T-test p-values were computed using non-parametric permutation and connectivity-based fixel enhancement to correct for multiple comparisons. Sex and age were set as covariates in the general linear model.

Wilcoxon-Mann-Whitney $p = 0.003$). Moreover, both patients and controls had a female prevalence (COVID-CM: 11/16; COVID-OD: 25/35; CTRL: 8/14). The possible impact of age and sex differences on the analysis was nevertheless accounted for by the statistical methods implemented. COVID-CM and COVID-OD patients underwent brain MRI at 293[212–367] and 251[208–286] days after disease onset, respectively.

Most patients (46/51) contracted the disease between February and April 2020 in Lombardy, the outbreak's epicentre during Italy's first and most severe wave of COVID-19, and before the vaccination campaign could reach them (Chirico et al., 2021).

3.2. Brain volumes

The morphological analysis revealed significant GM atrophy in COVID-CM as compared to CTRL patients (697[675–733] vs 757 [713–801] cm^3; sex, age, and BrainSegVol corrected $p = 0.004$) (Fig. 2). Although no overall GM atrophy was observed in COVID-OD patients, a significant reduction in the BrainSegVol-normalized volume ($p < 0.010$) was found in several individual GM regions after accounting for age and sex differences (Supplementary Table 2).

A significant reduction in average cortical thickness of the right hemisphere was observed in both COVID-19 patient groups (COVID-CM: 1.73[1.66–1.89] mm, COVID-OD: 1.99[1.78–2.24] mm, CTRL: 2.23 [1.93–2.41] mm; sex and age corrected $p < 0.001$). In both patient groups, the region-specific analysis showed a significant decrease in cortical thickness (sex and age corrected $p < 0.001$) in the posterior cingulate, isthmus cingulate, and parahippocampal cortex (Supplementary Table 3).

3.3. Brain microstructure

We found a significant overall GM MD increase in both COVID-CM and COVID-OD, as compared to CTRL patients (0.85[0.82–0.9] and 0.83[0.81–0.86] 10^3 mm^2/s vs. 0.80[0.78–0.83] 10^3 mm^2/s; sex, age, and BrainSegVol corrected $p = 0.001$) (Fig. 2). Brain GM regions with the highest MD alterations included the left and right frontal area, the right precentral, and both parietal regions (age and sex corrected $p \leq 0.001$, p adjusted for multiple comparisons < 0.050). The left precentral and right cuneus GM regions were also involved in COVID-OD patients (Table 2, Supplementary Fig. 2).

An overall WM MD increase was found in COVID-CM patients as compared with control patients (0.68[0.67–0.69] vs. 0.66[0.66–0.67] 10^3 mm^2/s; sex, age, and BrainSegVol corrected $p = 0.022$) (Fig. 2). At the WM regional level, a significant MD increase was found in the medulla, the posterior corona radiata, in the forceps minor of the corpus callosum (CC) bundle, and, in common with the COVID-OD group, in the right inferior and middle cerebellar peduncle (age and sex corrected $p < 0.001$, p adjusted for multiple comparisons < 0.050) (Table 2).

At the global level, the only significant FA alteration was found in the WM of COVID-CM patients ($p = 0.038$). However, after accounting for the effect of age, sex, and BrainSegVol, the alteration was no longer significant (Fig. 2). In the WM tissue, decreased FA was found in tracts within the medulla in COVID-CM patients, plus the middle cerebellar peduncle in the COVID-OD group (Table 2).

Supplementary Table 1 extends Table 2, reporting all statistically significant results, including those not remaining after multiple comparisons correction.

The tractometry on the major WM bundles confirmed the significant

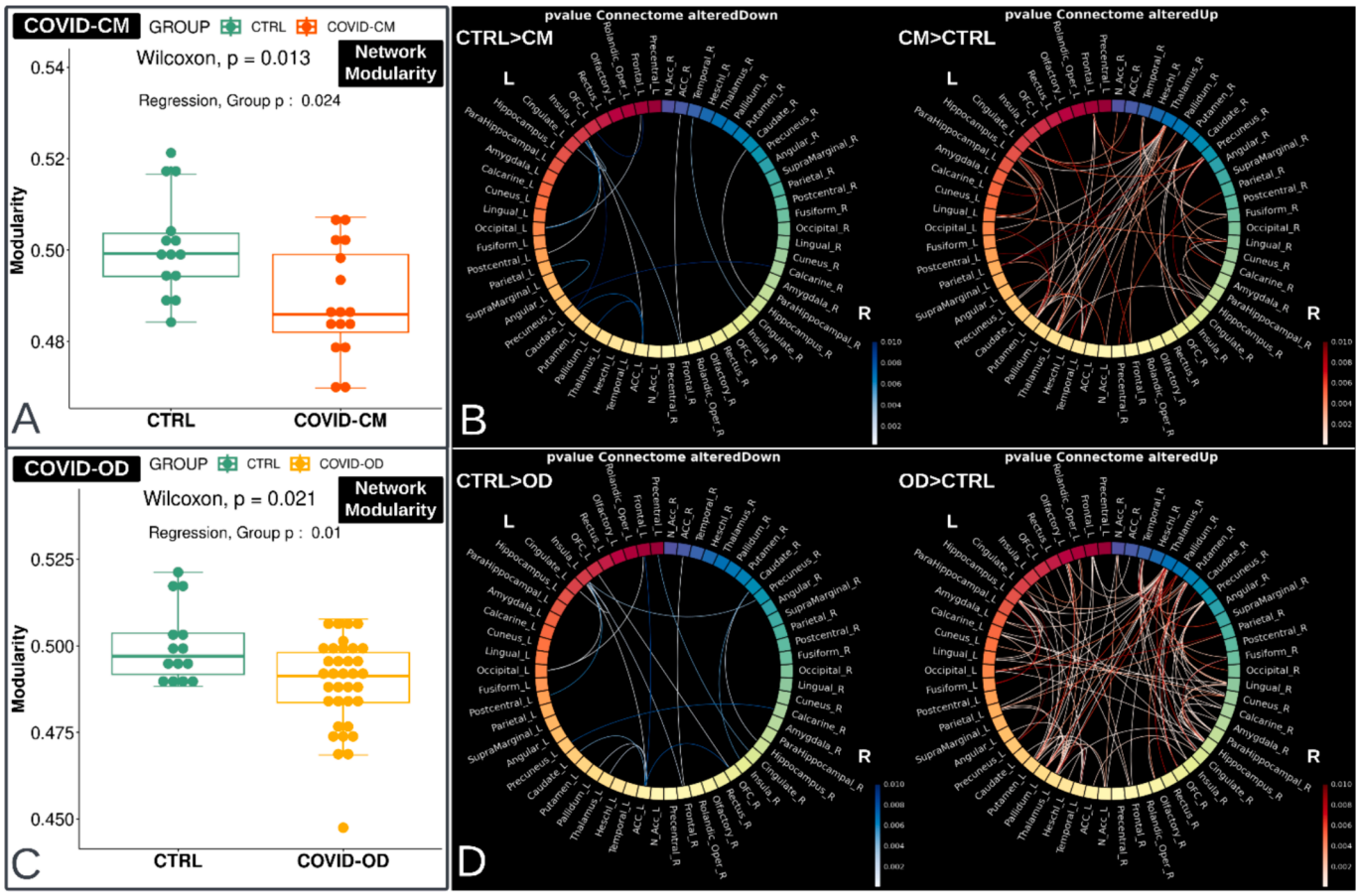

Fig. 4. Network modularity and connectome in COVID-19 patients with cognitive deficit (COVID-CM, n = 16, top) or olfactory disorder (COVID-OD, n = 35, bottom) as compared with normal controls (CTRL, n = 14). The figure's left side (boxplots A and C) displays the network modularity distribution, computed via the community detection Louvain method. The network comprises 58 gray matter regions derived from the AAL3 atlas, excluding the cerebellum, vermis, supplementary motor areas, and paracentral lobules. Wilcoxon-Mann-Whitney p-value is reported along with the result from *t*-test the regression model that also accounts for the sex, age, and brain volume of the subjects. The connectomes on the right side of the figure (panels B and D) show the connections with significantly altered strength ($p < 0.01$) and the direction of the alteration. Blue indicates the connections weakened in the COVID-19 patients. Connection-specific P-values were computed using the Wilcoxon-Mann-Whitney test.

increase in MD within the forceps minor section of the CC in COVID-CM patients, also resulting from the MD regional analysis, and highlighted a significant FA decrease in the right uncinate fasciculus (UF) in COVID-OD patients (sex and age-corrected $p < 0.001$, adjusted $p < 0.050$).

The analysis of the FDC also revealed several significant alterations (Fig. 3), predominantly localized in the left hemisphere and affecting common white matter pathways across both groups. Specifically, we observed alterations in segments of the arcuate fasciculus, the inferior occipitofrontal fasciculus, the inferior, middle and superior longitudinal fasciculi (SLF III), and the optic radiation. Additionally, a reduction in FDC was observed in the left cerebral peduncle, as well as in the pre-central and post-central white matter tracts. Notably, the corpus callosum exhibited significant involvement, with the forceps minor predominantly involved in COVID-OD patients and the forceps major in COVID-CM patients (sex and age-corrected p value adjusted for multiple comparisons, $p < 0.050$). Comparison of the specific alterations in FD (Supplementary Fig. 3) and FC (Supplementary Fig. 4) reveals that the forceps major of the corpus callosum is significantly affected by a reduction in FD, while alterations in other bundles primarily originate from a substantial reduction in FC.

3.4. Brain connectivity

An overall increase in connectivity was observed in both patient groups, in conjunction with a more localized reduction in a few connections, mainly in the left hemisphere (Fig. 4). The significantly impaired connections ($p < 0.010$), defined by the two GM regions located at the WM bundle ends, are reported in Table 3.

In both COVID-CM and COVID-OD patients, as compared with the CTRL group, the overall increase in connectivity was associated with a significant reduction in network modularity (age, sex, and BrainSegVol corrected $p = 0.024$ and $p = 0.010$, respectively) (Fig. 4).

Table 4 displays differences in local connectivity measures between COVID-19 subgroups and CTRL patients. Both COVID-19 patient subgroups showed increased clustering coefficient and local efficiency in the right parahippocampal region and a decrease in the connectivity degree in the insula (age and sex-corrected $p < 0.001$, p adjusted for multiple comparisons < 0.050). In addition, COVID-CM patients showed significant connectivity strengthening in the right lingual region. Instead, COVID-OD patients exhibited increased connectivity in the left hippocampus, putamen, right thalamus, and parahippocampal region and decreased connectivity degree of the left OFC.

In COVID-CM patients, the NBS approach showed significant involvement of 5 connections (edges) and 6 GM regions (nodes) ($p = 0.014$), namely the left insula, cingulate, and postcentral region, the right frontal area, and both ACC regions. In COVID-OD patients, the same method revealed significant involvement of 6 edges and 7 GM nodes ($p = 0.026$), entirely located in the brain's left hemisphere, namely the left insula, cingulate, and ACC, like in COVID-CM patients, plus supramarginal, nucleus accumbens (N Acc), and occipital areas.

Table 3
Significantly impaired connections (p < 0.010) in COVID-19 patients with cognitive and memory deficit (COVID-CM, n = 16) or olfactory disorder (COVID-OD, n = 35) as compared with normal controls (CTRL, n = 14). The distribution of the differences is displayed as median [IQR] and compares the connections' weight. The U statistic and P-value were computed using the Wilcoxon-Mann-Whitney test. Abbreviations: ACC: anterior cingulate cortex; OFC: orbitofrontal cortex.

Significant impaired connections	COVID-CM	CTRL	U	p
Insula L – Postcentral L	0[0–517]	646[610–786]	25	<0.001
Caudate R – Hippocampus R	57[0–67]	131[122–156]	26	<0.001
ACC R – Frontal R	3099 [2501–4059]	4871 [4328–5221]	26	<0.001
Insula L – ACC L	0[0–0]	151[30–236]	39	<0.001
Frontal L – Occipital L	0[0–0]	333[0–461]	48	0.002
Insula L – Frontal R	0[0–0]	275[0–347]	50	0.004
Insula L – Cingulate L	0[0–80]	156[89–215]	46	0.004
Cingulate R – Temporal R	281[0–343]	384[347–477]	43	0.004
Angular L – Parietal L	2580 [2353–3053]	3460 [3164–4247]	45	0.006
Occipital L – Insula L	0[0–0]	295[0–349]	54	0.006
Caudate L – ACC L	160[70–206]	242[225–349]	47	0.007
Pallidum L – ACC L	0[0–0]	49[0–145]	62	0.008
Precuneus L – Calcarine R	48[0–78]	80[70–106]	49	0.009
OFC L – Frontal L	3563 [3122–3945]	4508 [4124–4719]	49	0.009
Insula L – Caudate L	0[0–62]	283[42–423]	54	0.009
Significant impaired connections	**COVID-OD**	**CTRL**	**U**	**p**
Frontal L – Occipital L	0[0–0]	333[0–461]	92	<0.001
ACC R – Frontal R	3056 [2726–3481]	4871 [4328–5221]	37	<0.001
Insula L – ACC L	0[0–0]	151[30–236]	86	<0.001
Insula L – Occipital L	0[0–0]	295[0–349]	107	<0.001
OFC R – OFC L	0[0–120]	181[113–263]	98	<0.001
Insula L – Cingulate L	0[0–72]	156[89–215]	102	<0.001
Caudate R – Hippocampus R	60[0–121]	131[122–156]	100	0.001
ACC L – Pallidum L	0[0–0]	49[0–145]	140	0.001
Insula L – Frontal R	0[0–62]	275[0–347]	124	0.002
ACC L – Thalamus L	75[0–131]	187[117–235]	110	0.002
Insula L – Precuneus R	0[0–0]	50[0–71]	133	0.004
ACC L – Caudate L	187[99–219]	242[225–349]	116	0.004
Cingulate R – Precentral L	133[0–160]	182[156–199]	118	0.005
Insula R – Caudate R	0[0–195]	232[53–328]	130	0.005
Postcentral L – Insula L	460[0–647]	646[610–786]	122	0.006
Precuneus L – Calcarine R	56[0–80]	80[70–106]	124	0.007
ACC L – OFC R	0[0–104]	139[109–214]	129	0.007
Frontal L – ACC L	3412 [3080–3922]	3933 [3652–4160]	125	0.008

The left insula was primarily involved in the altered connectivity subnetworks, being part of 4 out of 5 impaired connections for COVID-CM patients and 4 out of 6 ones in the COVID-OD group.

Fig. 5 shows the altered connectivity subnetworks and the output of the graph-based analysis restricted to these subnetworks. Both the patient groups exhibited a decrease in the connectome's density. In addition, COVID-CM patients showed more modules and lower global efficiency, while COVID-OD patients showed increased modularity (sex, age, and BrainSegVol corrected $p < 0.050$). Supplementary Fig. 2 visually depicts, by color-coded overlay on a T1-weighted scan, the alterations in brain connectivity and GM microstructure.

Additionally, we evaluated microstructure along the affected fibers, finding a significant MD increase in COVID-CM patients (sex and age-corrected $p = 0.001$).

4. Discussion

This study showed significant alterations in brain morphology, microstructure, and connectivity in COVID-19 patients with olfactory dysfunction or cognitive deficits compared to control patients.

GM atrophy was measured locally in COVID-19 patients, especially in the COVID-CM group, where the overall tissue was reduced. Furthermore, the morphological analysis showed mild cortical thinning in both COVID-19 patient groups, mainly involving the posterior cingulate, isthmus cingulate, and parahippocampal cortex. These findings align with previous evidence and may underlie neurological impairment (Douaud et al., 2022; Rothstein, 2023; Sanabria-Diaz et al., 2022), particularly associated with memory, attention, and olfaction, consistent with the deficits observed in the patients (Aminoff et al., 2013; De Luca et al., 2022; Hugon et al., 2022). The cortical thinning in the parahippocampal gyrus is especially in line with prior research and the olfactory and memory impairment (De Luca et al., 2022; Douaud et al., 2022).

Regarding brain microstructure, patients showed increased MD in the GM compared with controls. The result concurs with studies showing increased diffusivity in COVID-19 patients, particularly those with neurological manifestations (Caroli et al., 2023; Douaud et al., 2022). The regions with the highest MD increase were the frontal, precentral, and parietal. COVID-OD patients additionally showed MD alterations in the right cuneus. These areas emerged as altered in previous evidence (Alhazmi et al., 2023; Kandemirli et al., 2020; Teller et al., 2022; Toniolo et al., 2021).

An increase in GM MD indicates higher water molecule diffusion within the tissue, possibly due to underlying processes, such as neuronal damage. In the case of COVID-19 disease, a direct brain viral invasion or the indirect effects of systemic inflammation can explain the neuronal injury (Bayat et al., 2022; Boroujeni et al., 2021). Also, the hypoxia caused by COVID-19-related respiratory difficulties or vascular complications may contribute to tissue damage by affecting cellular metabolism and, eventually, the integrity of neurons. Such pathological processes are also coherent with the observed GM atrophy and might be ushering to abnormal cognitive or sensory functions (Alqahtani et al., 2023).

Similarly, the overall WM MD increase found in COVID-CM patients, and the local WM MD increase observed in both patient groups could imply neuronal damage via disrupted axonal integrity, demyelination, axonal loss, and vasogenic edema (Rau et al., 2022). Affected regions include the inferior and middle cerebellar peduncle, medulla, posterior corona radiata, and forceps minor of the CC. Tractometry also detected alterations in the UF bundle in COVID-OD patients (Caroli et al., 2023).

The right cerebellar peduncle showed increased diffusivity in both COVID-CM and COVID-OD patients. Since the cerebellum is involved in cognitive functions, damage in the peduncle may reflect disruptions in the communication pathways to other brain regions, contributing to the pertinent symptoms' onset (Grossauer et al., 2015; Tobyne et al., 2018).

The MD increase in the forceps minor is coherent with studies finding increased radial diffusivity and reduced apparent fiber density in CC, UF, and corona radiata (Bispo et al., 2022; Campabadal et al., 2022). Furthermore, an MD increase in the forceps minor was previously associated with mild cognitive impairment, providing valuable insights to distinguish the amnestic subtype from that caused by cerebral small vessel disease (Y. Zhang et al., 2022).

However, increased diffusivity in the WM, potentially due to vasogenic edema, is controversial in COVID-19 literature (Rau et al., 2022). Indeed, few studies found diffusion restriction (Altmann et al., 2022; Rasmussen et al., 2020) and the presence of cerebral microbleeds (CMB) in the same areas (Napolitano et al., 2022), likely due to the activation of the cytokine storm and subsequent cytotoxic edema. One key aspect to consider is the timing of MRI imaging relative to disease onset. Studies reporting cytotoxic edema involve imaging in the acute or subacute phases of COVID-19, whereas this study examined patients at

Table 4

Significantly altered measures of local connectivity (p < 0.010), namely clustering coefficient (clusterCoeff), degree, local efficiency, and strength, in the brain network of COVID-19 patients with cognitive and memory deficit (COVID-CM, n = 16) or olfactory disorder (COVID-OD, n = 35) as compared with normal controls (CTRL, n = 14). P-values were computed by *t*-test in a multiple linear regression estimated with a robust model also considering the age and sex of the subjects. Bold font indicates which differences stay significant (p adjusted < 0.050) after correcting for multiple comparisons via the Holm–Bonferroni method, accounting for 58 comparisons covering the gray matter network nodes. Abbreviations: OFC: orbitofrontal cortex.

Connectivity Measure	COVID-CM	CTRL	p	Direction
clusterCoeff ParaHippocampal R	**645 [562–930]**	**326 [237–389]**	**<0.001**	↑
clusterCoeff Insula L	677[396–781]	340[297–386]	0.001	↑
clusterCoeff Calcarine R	442[370–561]	336[289–355]	0.004	↑
clusterCoeff Fusiform L	1121[838–1325]	671[424–955]	0.004	↑
clusterCoeff Precuneus R	303[255–356]	226[221–246]	0.005	↑
clusterCoeff OFC R	630[463–726]	434[375–503]	0.007	↑
degree Insula L	**12 [9–14]**	**19 [15–22]**	**<0.001**	↓
degree Putamen R	34[31–36]	29[27–31]	0.006	↑
degree Fusiform L	6[5–6]	9[6–9]	0.010	↓
localEfficiency ParaHippocampal R	**724 [653–1010]**	**389 [283–478]**	**<0.001**	↑
localEfficiency Insula L	923[527–1023]	475[418–549]	0.002	↑
localEfficiency Fusiform L	1208[925–1519]	747[483–1044]	0.003	↑
localEfficiency Calcarine R	562[423–679]	411[374–451]	0.005	↑
localEfficiency Precuneus R	429[372–529]	343[313–353]	0.006	↑
strength Lingual R	**14948 [12398–17887]**	**10631 [9650–12028]**	**<0.001**	↑
strength ParaHippocampal R	7628[6250–10153]	5314[4950–6171]	0.004	↑
strength Thalamus R	21734[19766–23701]	18374[17698–19092]	0.004	↑
strength Fusiform R	14132[10938–16675]	9794[9498–11974]	0.005	↑
strength Putamen L	25734[22879–36000]	20610[20066–22284]	0.005	↑
Connectivity Measure	**COVID-OD**	**CTRL**	**p**	**Direction**
clusterCoeff ParaHippocampal R	**738 [545–921]**	**326 [237–389]**	**<0.001**	↑
clusterCoeff Insula L	642[464–837]	340[297–386]	0.002	↑
clusterCoeff ParaHippocampal L	569[456–796]	377[312–466]	0.002	↑
clusterCoeff OFC R	587[430–767]	434[375–503]	0.005	↑
degree Insula L	**11 [10–15]**	**19 [15–22]**	**<0.001**	↓
degree OFC L	**9 [8–11]**	**12 [11–13]**	**<0.001**	↓
degree Thalamus R	39[36–41]	36[32–38]	0.002	↑
degree Thalamus L	38[36–41]	35[31–40]	0.003	↑
degree Olfactory L	12[10–15]	8[7–10]	0.005	↑
localEfficiency ParaHippocampal R	**802 [612–1013]**	**389 [283–478]**	**<0.001**	↑
localEfficiency ParaHippocampal L	646[528–829]	432[379–547]	0.002	↑
localEfficiency OFC R	738[575–977]	583[465–677]	0.005	↑
localEfficiency Insula L	806[594–1016]	475[418–549]	0.005	↑
strength Hippocampus L	**11557 [10629–14151]**	**9422 [8740–9928]**	**<0.001**	↑
strength Putamen L	**26871 [24010–31724]**	**20610 [20066–22284]**	**<0.001**	↑
strength Thalamus R	**21081 [20146–24090]**	**18374 [17698–19092]**	**<0.001**	↑
strength ParaHippocampal R	**7223 [6166–10116]**	**5314 [4950–6171]**	**<0.001**	↑
strength Fusiform R	12767[11058–15388]	9794[9498–11974]	0.001	↑
strength Heschl L	2115[1892–2942]	1664[1309–2054]	0.001	↑
strength Precuneus R	18916[18370–23048]	16164[15776–17889]	0.003	↑
strength ParaHippocampal L	5678[5083–8373]	4832[4478–5224]	0.003	↑
strength Thalamus L	21897[20843–26258]	20213[18996–20886]	0.003	↑
strength Lingual R	13028[11836–16468]	10631[9650–12028]	0.004	↑
strength Olfactory R	2168[1740–2840]	1414[1190–1638]	0.009	↑
strength Hippocampus R	11725[10645–13187]	9024[8427–10224]	0.009	↑

significantly later time points. This temporal distinction may be crucial because cytotoxic edema has been observed to precede or accompany vasogenic edema in conditions such as traumatic brain injury (Lee et al., 2024) and acute ischemic stroke (X. Zhang et al., 2022). While there is a lack of direct evidence regarding the progression of edema from cytotoxic to vasogenic forms in COVID-19, the observed differences in MRI timing across studies suggest a possible temporal evolution of the process.

A substantial impact of the disease on the commissural fibers of the corpus callosum, including the forceps minor, is also suggested by fixel analysis and FDC assessment. However, the forceps major was involved in COVID-CM patients, while in COVID-OD patients, the forceps minor was mainly involved. Although not statistically significant when corrected for confounding factors, an overall FA reduction in the WM emerged in COVID-CM patients, potentially suggesting a higher impact on the axonal integrity in this group.

On the other hand, localized reductions in WM FA were significant in the medulla (in both COVID-19 groups) and in the middle cerebellar peduncle (in COVID-OD patients only). Medulla and cerebellar peduncle FA decrease aligns with the hypothesis of regional axonal disruptions suggested by the increased diffusivity. Among the WM tracts that showed significantly altered FDC, left-sided bundles implicated in attention, memory, and language processing emerged. These included the arcuate fasciculus and the inferior and superior longitudinal fasciculi (SLF III). These findings are notably consistent with the symptoms observed in the study population, particularly COVID-CM patients.

Additionally, WM pathways associated with visual processing, as well as motor and somatosensory functions, demonstrated involvement. The first is evidenced by alterations in the optic radiation and the inferior occipitofrontal fascicle, while the latter is suggested by the involvement of the cerebral peduncle as well as the pre-central and post-central regions, respectively. The involvement of the left cerebral peduncle is consistent with one of the very few past studies investigating fixel-based parameters in COVID-19 patients (Lathouwers et al., 2023).

Turning to structural connectivity, the graph-based assessment of the brain network revealed reduced network modularity in COVID-CM and COVID-OD patients, with an extensive pattern of connectivity increase and few specific decreased connections.

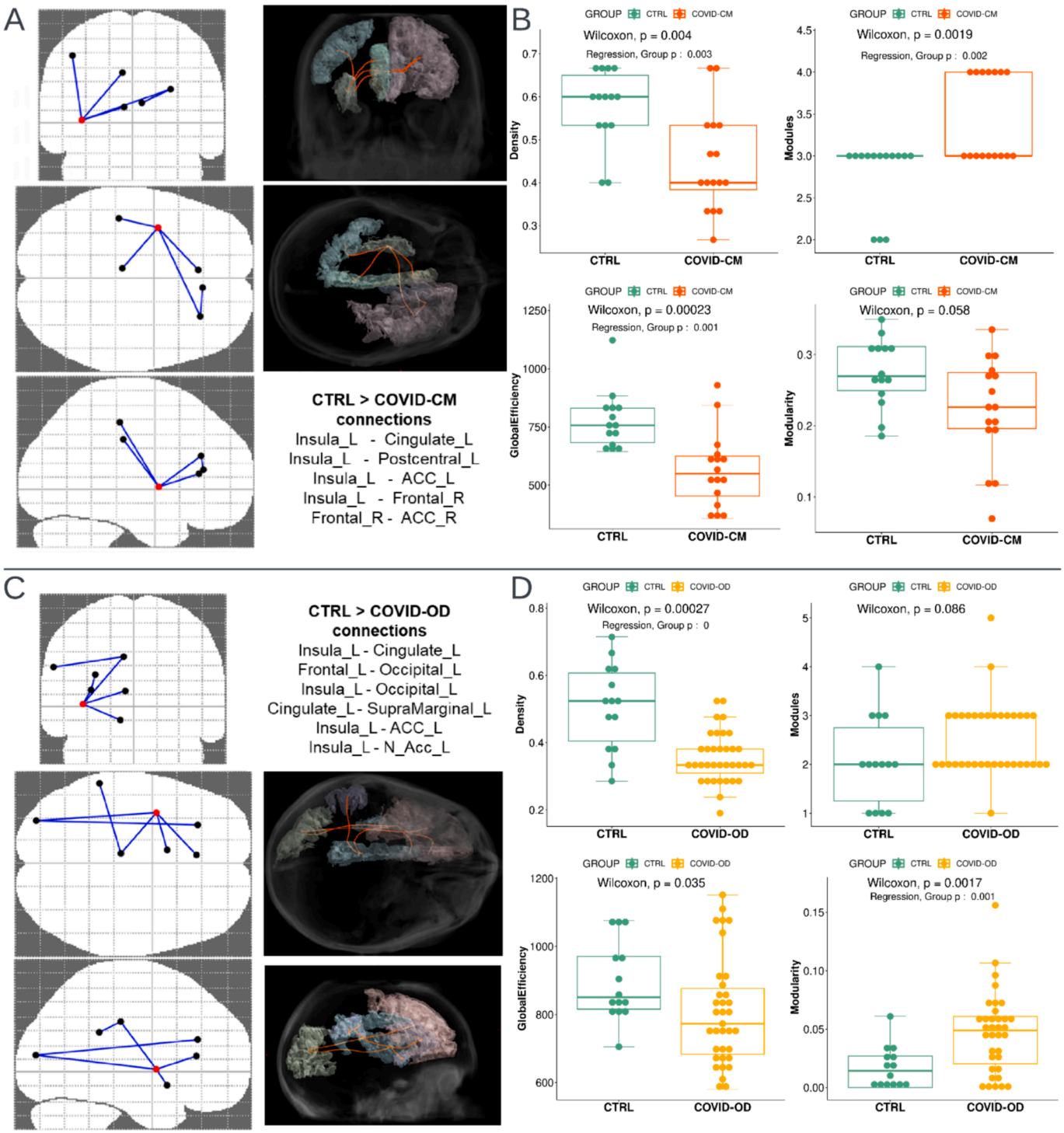

Fig. 5. Brain connection impairment in COVID-19 patients with cognitive (COVID-CM, n = 16, top) or olfactory disorder (COVID-OD, n = 35, bottom) as compared with normal controls (CTRL, n = 14). The left side of the figure shows the pattern and list of significantly impaired connections (A, C). The right side of the figure (boxplots B and D) shows the results of the connectivity analysis, and in particular, the distribution of the density, number of modules, modularity, and global efficiency of the gray matter subnetwork affected by the impaired connections. The significantly altered connections were identified and corrected for multiple comparisons using the Network-Based Statistics (NBS) tool t-tests and while taking into account the age and sex of the subjects. P-values for connectivity measures were computed using the Wilcoxon-Mann-Whitney test. T-test p-values of the group variable in the linear regression model accounting also for sex, age, and brain volume of the subjects are reported when significant ($p < 0.05$). Abbreviations: ACC: anterior cingulate cortex; N Acc: nucleus accumbens.

The loss of brain network specificity, to the advantage of structural hyperconnectivity, might be related to an ongoing compensatory mechanism. Past studies suggested functional hyperconnectivity as a response to neurological insults and neurodegeneration (Aswendt and Hoehn, 2022). Although the relationship between changes in functional and structural connectivity after brain injuries remains uncertain, recovery is believed to be linked to both remodelling, possibly involving neuronal plasticity due to dendritic morphology changes, synaptogenesis, and axonal sprouting (van Meer et al., 2012).

Decreased connectivity was primarily in the left hemisphere,

especially in COVID-OD patients, consistent with prior evidence indicating a foremost impact on this side of the brain (Douaud et al., 2022) and with the FDC result. Moreover, a previous functional MRI study found elevated levels of the amplitude of low-frequency fluctuations (ALFF) in the left hemisphere, namely in the insula, hippocampus, parahippocampal gyrus, postcentral gyrus, supramarginal gyrus, caudate, thalamus, and putamen, supporting the primary left-sided impairment and the hypothesis of a compensatory hyperconnectivity (Du et al., 2021).

The impaired subnetworks encompassed the left cingulate, ACC, and insula among the most affected GM regions in both COVID-OD and COVID-CM patient groups.

Other GM regions involved in the case of COVID-OD patients included the left N Acc, typically part of the olfactory subnetwork (Esposito et al., 2022; Muccioli et al., 2023), and the frontal, supramarginal, and occipital cortex. These findings are coherent with a previous functional MRI study in healthy volunteers showing olfactory-stimulated activation in the left insula, supramarginal gyrus, occipital cortex, and limbic areas, such as frontal, cingulate, and orbitofrontal cortex (Ciorba et al., 2021). In COVID-CM patients, impaired connections also involved the left post-central gyrus and right ACC and frontal area, already associated with metabolism, morphology, and functional connectivity alterations in COVID-19 (Douaud et al., 2022; Du et al., 2021; Kas et al., 2021; Sanabria-Diaz et al., 2022).

The prominent involvement of the left insula region in both patient groups aligns with previous evidence and is also consistent with the symptoms experienced by the groups. As mentioned, the insula plays a key role in olfaction but also deals with various cognitive and emotional functions; it directly connects to the primary olfactory cortex and serves as the primary gustatory cortex. Since the insula is also vital in processing subjective awareness and integrating homeostatic information, alterations are also expected to be implicated in the abnormal perception of respiratory failure reported in COVID-19 patients (Douaud et al., 2022; Kas et al., 2021).

The insula is also connected to other olfactory and cognitive processing regions, including the OFC, housing the secondary gustatory cortex and the secondary and tertiary olfactory regions (Rolls, 2004), amygdala, hippocampus, and ACC. The last is primarily linked with attention and working memory tasks (Douaud et al., 2022; García-Cabezas and Barbas, 2014; Kas et al., 2021) but is also associated with activating the primary olfactory cortex along the OFC (Ciorba et al., 2021; García-Cabezas and Barbas, 2014).

Local connectivity results, specifically the node's degree reduction, supported the disruption of connection routes involving the left insula for both patient groups and of the OFC for the COVID-OD patients.

The increased connection strength observed in the thalamus, hippocampus, parahippocampal region, and putamen is consistent with the presumed compensatory process and previous studies reporting functional hyperconnectivity in COVID-19 patients (Du et al., 2021), especially with olfactory disorders (Muccioli et al., 2023).

The study has limitations to be acknowledged. Firstly, the imaging protocol was sub-optimal, designed for clinical routine in an emergency, and included slight differences in acquisition parameters between patients and controls. The circumstance also did not allow an evaluation of cerebral dominance. Secondly, this was a retrospective and monocentric observational study with a relatively small sample size. Furthermore, pre-COVID-19 imaging data were unavailable. However, it is noteworthy that several results are consistent with findings in studies with larger cohorts and pre-infection imaging data. Last, no quantitative clinical variable was collected to test asymptomatic impairments and assess the severity of olfactory or cognitive disorders.

On the other hand, the methods were designed to address the imaging limitations and provide reliable processing. In particular, state-of-the-art routines for diffusion signal elaboration were applied. Moreover, to our knowledge, this study is one of the first to separately characterize COVID-19 patients exhibiting cognitive deficits or olfactory disorders and compare their alterations in structural connectivity through quantitative tractography and graph-based analysis. Furthermore, the study's population consisted of patients affected during the early stages of the COVID-19 outbreak, in a time and place where the pandemic struck the most in Italy.

5. Conclusions

In conclusion, this study showed significant brain alterations occurring at the morphology, microstructure, and structural connectivity levels in COVID-19 patients experiencing olfactory or cognitive impairment. These findings suggest the presence of underlying GM and WM neurodegeneration and neuroinflammation, as well as compensatory mechanisms, and provide insights into the affected brain regions.

Identifying the precise location and type of cerebral alterations can help elucidate the origins of the symptoms and the pathological mechanisms triggered by COVID-19 in the brain.

Future longitudinal studies are needed to monitor COVID-19 brain alterations and ultimately assess their transient or permanent nature.

CRediT authorship contribution statement

Alberto Arrigoni: Writing – original draft, Methodology, Investigation, Formal analysis, Data curation, Conceptualization. **Mattia Previtali:** Writing – review & editing, Methodology, Data curation. **Sara Bosticardo:** Writing – review & editing, Methodology, Investigation. **Giulio Pezzetti:** Writing – review & editing, Investigation, Data curation. **Sofia Poloni:** Writing – review & editing, Methodology. **Serena Capelli:** Writing – review & editing, Investigation, Data curation. **Angela Napolitano:** Writing – review & editing, Investigation, Data curation. **Andrea Remuzzi:** Writing – review & editing, Investigation. **Rosalia Zangari:** Writing – review & editing, Investigation. **Ferdinando Luca Lorini:** Writing – review & editing, Investigation. **Maria Sessa:** Writing – review & editing, Investigation. **Alessandro Daducci:** Writing – review & editing, Supervision, Methodology, Investigation. **Anna Caroli:** Writing – original draft, Supervision, Methodology, Investigation, Formal analysis, Data curation, Conceptualization. **Simonetta Gerevini:** Writing – review & editing, Supervision, Investigation, Conceptualization.

Declaration of Competing Interest

The authors declare that they have no known competing financial interests or personal relationships that could have appeared to influence the work reported in this paper.

Data availability

Data will be made available on request.

Acknowledgements

The authors gratefully acknowledge Cristina Casalini, radiology technician, for acquisition of most MRIs in the first part of the pandemic, Carmelo Parisi, MR zone clinical leader for setting of the imaging sequences, nurses, and technicians of Neuroradiology Unit for devotion and support in managing these patients especially at the beginning of the pandemic.

The study was supported in part by a grant from Brembo SpA (Curno, Bergamo, Italy), under the initiative "Progetto TrexUno". Dr A. Arrigoni received a scholarship from "Aiuti per la Ricerca sulle Malattie Rare" (A.R.M.R) Foundation.

Data availability.

The data that support the findings of this study are available from the corresponding author, upon reasonable request.

Ethics approval statement.

The study was conducted in accordance with the Declaration of Helsinki and approved by the local Institutional Review Board (Comitato Etico di Bergamo, Italy) within the framework of the observational study protocol Reg. 118/22 (21/07/2022).

Informed Consent Statement.

Informed consent was obtained from patients or their next of kin.

Appendix A. Supplementary data

Supplementary data to this article can be found online at https://doi.org/10.1016/j.nicl.2024.103631.

References

Alhazmi, F.H., Alsharif, W.M., Alshoabi, S.A., Gameraddin, M., Aloufi, K.M., Abdulaal, O. M., Qurashi, A.A., 2023. Identifying cerebral microstructural changes in patients with COVID-19 using MRI: A systematic review. Brain Circ 9, 6–15. https://doi.org/10.4103/bc.bc_77_22.

Alqahtani, M.S., Abbas, M., Alshahrani, M.Y., Alabdullh, K., Alqarni, A., Alqahtani, F.F., Jambi, L.K., Alkhayat, A., 2023. Effects of COVID-19 on Synaptic and Neuronal Degeneration. Brain Sciences 13, 131. https://doi.org/10.3390/brainsci13010131.

Altmann, K., Koziol, K., Palaver, A., Frisch, G., Pfausler, B., Helbok, R., Kampfl, A., 2022. Cytotoxic Edema Involving the Corpus Callosum and Middle Cerebellar Peduncles in a Young Patient With Mild COVID-19. Neurology 99, 115–116. https://doi.org/10.1212/WNL.0000000000200816.

Aminoff, E.M., Kveraga, K., Bar, M., 2013. The role of the parahippocampal cortex in cognition. Trends Cogn Sci 17, 379–390. https://doi.org/10.1016/j.tics.2013.06.009.

Assaf, Y., Pasternak, O., 2008. Diffusion Tensor Imaging (DTI)-based White Matter Mapping in Brain Research: A Review. J Mol Neurosci 34, 51–61. https://doi.org/10.1007/s12031-007-0029-0.

Aswendt, M., Hoehn, M., 2022. Functional hyperconnectivity related to brain disease: maladaptive process or element of resilience? Neural Regen Res 18, 1489–1490. https://doi.org/10.4103/1673-5374.361541.

Bayat, A.-H., Azimi, H., Hassani Moghaddam, M., Ebrahimi, V., Fathi, M., Vakili, K., Mahmoudiasl, G.-R., Forouzesh, M., Boroujeni, M.E., Nariman, Z., Abbaszadeh, H.-A., Aryan, A., Aliaghaei, A., Abdollahifar, M.-A., 2022. COVID-19 causes neuronal degeneration and reduces neurogenesis in human hippocampus. Apoptosis 27, 852–868. https://doi.org/10.1007/s10495-022-01754-9.

Boroujeni, M.E., Simani, L., Bluyssen, H.A.R., Samadikhah, H.R., Zamanlui Benisi, S., Hassani, S., Akbari Dilmaghani, N., Fathi, M., Vakili, K., Mahmoudiasl, G.-R., Abbaszadeh, H.A., Hassani Moghaddam, M., Abdollahifar, M.-A., Aliaghaei, A., 2021. Inflammatory Response Leads to Neuronal Death in Human Post-Mortem Cerebral Cortex in Patients with COVID-19. ACS Chem Neurosci 12, 2143–2150. https://doi.org/10.1021/acschemneuro.1c00111.

Campabadal, A., Oltra, J., Junqué, C., Guillen, N., Botí, M.Á., Sala-Llonch, R., Monté-Rubio, G.C., Lledó, G., Bargalló, N., Rami, L., Sánchez-Valle, R., Segura, B., 2022. Structural brain changes in post-acute COVID-19 patients with persistent olfactory dysfunction. Ann Clin Transl Neurol 10, 195–203. https://doi.org/10.1002/acn3.51710.

Capelli, S., Caroli, A., Barletta, A., Arrigoni, A., Napolitano, A., Pezzetti, G., Longhi, L.G., Zangari, R., Lorini, F.L., Sessa, M., Remuzzi, A., Gerevini, S., 2023. MRI evidence of olfactory system alterations in patients with COVID-19 and neurological symptoms. J Neurol 270, 1195–1206. https://doi.org/10.1007/s00415-023-11561-0.

Caroli, A., Capelli, S., Napolitano, A., Cabrini, G., Arrigoni, A., Pezzetti, G., Previtali, M., Longhi, L.G., Zangari, R., Lorini, F.L., Sessa, M., Remuzzi, A., Gerevini, S., 2023. Brain diffusion alterations in patients with COVID-19 pathology and neurological manifestations. Neuroimage Clin 37, 103338. https://doi.org/10.1016/j.nicl.2023.103338.

Chirico, F., Nucera, G., Szarpak, L., 2021. COVID-19 mortality in Italy: The first wave was more severe and deadly, but only in Lombardy region. Journal of Infection 83, e16.

Ciorba, A., Hatzopoulos, S., Cogliandolo, C., Bianchini, C., Renna, M., Perrucci, L., Skarzynska, M., Skarżyński, P.H., Campioni, P., Cittanti, C., Carnevale, A., Giganti, M., Pelucchi, S., 2021. Functional Magnetic Resonance Imaging in the Olfactory Perception of the Same Stimuli. Life 11, 11. https://doi.org/10.3390/life11010011.

Davis, H.E., Assaf, G.S., McCorkell, L., Wei, H., Low, R.J., Re'em, Y., Redfield, S., Austin, J.P., Akrami, A., 2021. Characterizing long COVID in an international cohort: 7 months of symptoms and their impact. eClinicalMedicine 38. https://doi.org/10.1016/j.eclinm.2021.101019.

Bispo, D.D. de C., Brandão, P.R. de P., Pereira, D.A., Maluf, F.B., Dias, B.A., Paranhos, H. R., von Glehn, F., de Oliveira, A.C.P., Soares, A.A. de S.M., Descoteaux, M., Regattieri, N.A.T., 2023. Altered structural connectivity in olfactory disfunction after mild COVID-19 using probabilistic tractography. Sci Rep 13, 12886. https://doi.org/10.1038/s41598-023-40115-7.

Bispo, D.D. de C., Brandão, P.R. de P., Pereira, D.A., Maluf, F.B., Dias, B.A., Paranhos, H. R., von Glehn, F., de Oliveira, A.C.P., Regattieri, N.A.T., Silva, L.S., Yasuda, C.L., Soares, A.A. de S.M., Descoteaux, M., 2022. Brain microstructural changes and fatigue after COVID-19. Frontiers in Neurology 13.

De Luca, P., Marra, P., La Mantia, I., Salzano, F.A., Camaioni, A., Di Stadio, A., 2022. Entorhinal Cortex and Persistent Olfactory Loss in COVID-19 Patients: A Neuroanatomical Hypothesis. Comment on Fiorentino et al. Correlations between Persistent Olfactory and Semantic Memory Disorders after SARS-CoV-2 Infection. Brain Sci. 2022, 12, 714. Brain Sci 12, 850. https://doi.org/10.3390/brainsci12070850.

Dhollander, T., Clemente, A., Singh, M., Boonstra, F., Civier, O., Duque, J.D., Egorova, N., Enticott, P., Fuelscher, I., Gajamange, S., Genc, S., Gottlieb, E., Hyde, C., Imms, P., Kelly, C., Kirkovski, M., Kolbe, S., Liang, X., Malhotra, A., Mito, R., Poudel, G., Silk, T.J., Vaughan, D.N., Zanin, J., Raffelt, D., Caeyenberghs, K., 2021. Fixel-based Analysis of Diffusion MRI: Methods, Applications. Challenges and Opportunities. Neuroimage 241, 118417. https://doi.org/10.1016/j.neuroimage.2021.118417.

Douaud, G., Lee, S., Alfaro-Almagro, F., Arthofer, C., Wang, C., McCarthy, P., Lange, F., Andersson, J.L.R., Griffanti, L., Duff, E., Jbabdi, S., Taschler, B., Keating, P., Winkler, A.M., Collins, R., Matthews, P.M., Allen, N., Miller, K.L., Nichols, T.E., Smith, S.M., 2022. SARS-CoV-2 is associated with changes in brain structure in UK Biobank. Nature 604, 697–707. https://doi.org/10.1038/s41586-022-04569-5.

Du, Y.-Y., Zhao, W., Zhou, X.-L., Zeng, M., Yang, D.-H., Xie, X.-Z., Huang, S.-H., Jiang, Y.-J., Yang, W.-H., Guo, H., Sun, H., Liu, J.-Y., Liu, P., Zhou, Z.-G., Luo, H., Liu, J., 2021. Survivors of COVID-19 exhibit altered amplitudes of low frequency fluctuation in the brain: a resting-state functional magnetic resonance imaging study at 1-year follow-up. Neural Regen Res 17, 1576–1581. https://doi.org/10.4103/1673-5374.327361.

Esposito, F., Cirillo, M., De Micco, R., Caiazzo, G., Siciliano, M., Russo, A.G., Monari, C., Coppola, N., Tedeschi, G., Tessitore, A., 2022. Olfactory loss and brain connectivity after COVID-19. Hum Brain Mapp 43, 1548–1560. https://doi.org/10.1002/hbm.25741.

Gabusi, I., Battocchio, M., Bosticardo, S., Schiavi, S., Daducci, A., 2024. Blurred streamlines: A novel representation to reduce redundancy in tractography. Medical Image Analysis 93, 103101. https://doi.org/10.1016/j.media.2024.103101.

García-Cabezas, M.Á., Barbas, H., 2014. A direct anterior cingulate pathway to the primate primary olfactory cortex may control attention to olfaction. Brain Struct Funct 219, 1735–1754. https://doi.org/10.1007/s00429-013-0598-3.

Grossauer, S., Koeck, K., Kau, T., Weber, J., Vince, G.H., 2015. Behavioral disorders and cognitive impairment associated with cerebellar lesions. J Mol Psychiatry 3, 5. https://doi.org/10.1186/s40303-015-0009-1.

Guo, P., Benito Ballesteros, A., Yeung, S.P., Liu, R., Saha, A., Curtis, L., Kaser, M., Haggard, M.P., Cheke, L.G., 2022. COVCOG 2: Cognitive and Memory Deficits in Long COVID: A Second Publication From the COVID and Cognition Study. Frontiers in Aging Neuroscience 14.

Hugon, J., Msika, E.-F., Queneau, M., Farid, K., Paquet, C., 2022. Long COVID: cognitive complaints (brain fog) and dysfunction of the cingulate cortex. J Neurol 269, 44–46. https://doi.org/10.1007/s00415-021-10655-x.

Kandemirli, S.G., Dogan, L., Sarikaya, Z.T., Kara, S., Akinci, C., Kaya, D., Kaya, Y., Yildirim, D., Tuzuner, F., Yildirim, M.S., Ozluk, E., Gucyetmez, B., Karaarslan, E., Koyluoglu, I., Demirel Kaya, H.S., Mammadov, O., Kisa Ozdemir, I., Afsar, N., Citci Yalcinkaya, B., Rasimoglu, S., Guduk, D.E., Kedir Jima, A., Ilksoz, A., Ersoz, V., Yonca Eren, M., Celtik, N., Arslan, S., Korkmazer, B., Dincer, S.S., Gulek, E., Dikmen, I., Yazici, M., Unsal, S., Ljama, T., Demirel, I., Ayyildiz, A., Kesimci, I., Bolsoy Deveci, S., Tutuncu, M., Kizilkilic, O., Telci, L., Zengin, R., Dincer, A., Akinci, I.O., Kocer, N., 2020. Brain MRI Findings in Patients in the Intensive Care Unit with COVID-19 Infection. Radiology 297, E232–E235. https://doi.org/10.1148/radiol.2020201697.

Karamali, K., Elliott, M., Hopkins, C., 2022. COVID-19 related olfactory dysfunction. Curr Opin Otolaryngol Head Neck Surg 30, 19–25. https://doi.org/10.1097/MOO.0000000000000783.

Kas, A., Soret, M., Pyatigoskaya, N., Habert, M.-O., Hesters, A., Le Guennec, L., Paccoud, O., Bombois, S., Delorme, C., on the behalf of CoCo-Neurosciences study group and COVID SMIT PSL study group, 2021. The cerebral network of COVID-19-related encephalopathy: a longitudinal voxel-based 18F-FDG-PET study. Eur J Nucl Med Mol Imaging 48, 2543–2557. https://doi.org/10.1007/s00259-020-05178-y.

Lathouwers, E., Radwan, A., Blommaert, J., Stas, L., Tassignon, B., Allard, S.D., De Ridder, F., De Waele, E., Hoornaert, N., Lacor, P., Mertens, R., Naeyaert, M., Raeymaekers, H., Seyler, L., Vanbinst, A.-M., Van Liedekerke, L., Van Schependom, J., Van Schuerbeek, P., Provyn, S., Roelands, B., Vandekerckhove, M., Meeusen, R., Sunaert, S., Nagels, G., De Mey, J., De Pauw, K., 2023. A cross-sectional case–control study on the structural connectome in recovered hospitalized COVID-19 patients. Sci Rep 13, 15668. https://doi.org/10.1038/s41598-023-42429-y.

Lechien, J.R., Vaira, L.A., Saussez, S., 2023. Prevalence and 24-month recovery of olfactory dysfunction in COVID-19 patients: A multicentre prospective study. Journal of Internal Medicine 293, 82–90. https://doi.org/10.1111/joim.13564.

Lee, J., Baniewicz, E., Peterkin, N.L., Greenman, D., Griffin, A.D., Jikaria, N., Turtzo, L. C., Luby, M., Latour, L.L., 2024. Edema progression in proximity to traumatic microbleeds: evolution of cytotoxic and vasogenic edema on serial MRI. Neuroimage Rep 4, 100199. https://doi.org/10.1016/j.ynirp.2024.100199.

Lou, J.J., Movassaghi, M., Gordy, D., Olson, M.G., Zhang, T., Khurana, M.S., Chen, Z., Perez-Rosendahl, M., Thammachantha, S., Singer, E.J., Magaki, S.D., Vinters, H.V., Yong, W.H., 2021. Neuropathology of COVID-19 (neuro-COVID): clinicopathological update. Free Neuropathol 2, 2. https://doi.org/10.17879/freeneuropathology-2021-2993.

Muccioli, L., Sighinolfi, G., Mitolo, M., Ferri, L., Jane Rochat, M., Pensato, U., Taruffi, L., Testa, C., Masullo, M., Cortelli, P., Lodi, R., Liguori, R., Tonon, C., Bisulli, F., 2023. Cognitive and functional connectivity impairment in post-COVID-19 olfactory dysfunction. NeuroImage: Clinical 38, 103410. https://doi.org/10.1016/j.nicl.2023.103410.

Napolitano, A., Arrigoni, A., Caroli, A., Cava, M., Remuzzi, A., Longhi, L.G., Barletta, A., Zangari, R., Lorini, F.L., Sessa, M., Gerevini, S., 2022. Cerebral Microbleeds

Assessment and Quantification in COVID-19 Patients With Neurological Manifestations. Front Neurol 13, 884449. https://doi.org/10.3389/fneur.2022.884449.

Rasmussen, C., Niculescu, I., Patel, S., Krishnan, A., 2020. COVID-19 and Involvement of the Corpus Callosum: Potential Effect of the Cytokine Storm? American Journal of Neuroradiology. https://doi.org/10.3174/ajnr.A6680.

Rau, A., Schroeter, N., Blazhenets, G., Dressing, A., Walter, L.I., Kellner, E., Bormann, T., Mast, H., Wagner, D., Urbach, H., Weiller, C., Meyer, P.T., Reisert, M., Hosp, J.A., 2022. Widespread white matter oedema in subacute COVID-19 patients with neurological symptoms. Brain 145, 3203–3213. https://doi.org/10.1093/brain/awac045.

Rolls, E.T., 2004. The functions of the orbitofrontal cortex. Brain Cogn 55, 11–29. https://doi.org/10.1016/S0278-2626(03)00277-X.

Rothstein, T.L., 2023. Cortical Grey matter volume depletion links to neurological sequelae in post COVID-19 "long haulers". BMC Neurology 23, 22. https://doi.org/10.1186/s12883-023-03049-1.

Rubinov, M., Sporns, O., 2010. Complex network measures of brain connectivity: uses and interpretations. Neuroimage 52, 1059–1069. https://doi.org/10.1016/j.neuroimage.2009.10.003.

Sanabria-Diaz, G., Etter, M.M., Melie-Garcia, L., Lieb, J.M., Psychogios, M.-N., Hutter, G., Granziera, C., 2022. Brain cortical alterations in COVID-19 patients with neurological symptoms. Frontiers in Neuroscience 16.

Sarafoleanu, C., Mella, C., Georgescu, M., Perederco, C., 2009. The importance of the olfactory sense in the human behavior and evolution. J Med Life 2, 196–198.

Schiavi, S., Ocampo-Pineda, M., Barakovic, M., Petit, L., Descoteaux, M., Thiran, J.-P., Daducci, A., 2020. A new method for accurate in vivo mapping of human brain connections using microstructural and anatomical information. Sci Adv 6, eaba8245. https://doi.org/10.1126/sciadv.aba8245.

Tassignon, B., Radwan, A., Blommaert, J., Stas, L., Allard, S.D., De Ridder, F., De Waele, E., Bulnes, L.C., Hoornaert, N., Lacor, P., Lathouwers, E., Mertens, R., Naeyaert, M., Raeymaekers, H., Seyler, L., Van Binst, A.M., Van Imschoot, L., Van Liedekerke, L., Van Schependom, J., Van Schuerbeek, P., Vandekerckhove, M., Meeusen, R., Sunaert, S., Nagels, G., De Mey, J., De Pauw, K., 2023. Longitudinal changes in global structural brain connectivity and cognitive performance in former hospitalized COVID-19 survivors: an exploratory study. Exp Brain Res 241, 727–741. https://doi.org/10.1007/s00221-023-06545-5.

Teller, N., Chad, J.A., Roudaia, E., Hashemi, A., Grosbein, H., Gilboa, A., Goubran, M., Cheng, I., Black, S.E., Fowler, R., Heyn, C., Gao, F., Masellis, M., Rabin, J., Ji, X., Jegatheesan, A., Lam, B., Sekuler, A.B., MacIntosh, B.J., Graham, S.J., Chen, J.J., 2022. "Long-hauler" impact of COVID-19 on brain microstructure: a 3-month follow-up study (P1-1.Virtual). Neurology 98.

Tobyne, S., Ochoa, W., Bireley, J., Smith, V., Geurts, J., Schmahmann, J., Klawiter, E., 2018. Cognitive Impairment and the Regional Distribution of Cerebellar Lesions in Multiple Sclerosis. Mult Scler 24, 1687–1695. https://doi.org/10.1177/1352458517730132.

Toniolo, S., Di Lorenzo, F., Scarioni, M., Frederiksen, K.S., Nobili, F., 2021. Is the Frontal Lobe the Primary Target of SARS-CoV-2? Journal of Alzheimer's Disease 81, 75–81. https://doi.org/10.3233/JAD-210008.

Tournier, J.-D., Calamante, F., Gadian, D.G., Connelly, A., 2004. Direct estimation of the fiber orientation density function from diffusion-weighted MRI data using spherical deconvolution. Neuroimage 23, 1176–1185. https://doi.org/10.1016/j.neuroimage.2004.07.037.

van Meer, M.P.A., Otte, W.M., van der Marel, K., Nijboer, C.H., Kavelaars, A., van der Sprenkel, J.W.B., Viergever, M.A., Dijkhuizen, R.M., 2012. Extent of Bilateral Neuronal Network Reorganization and Functional Recovery in Relation to Stroke Severity. J Neurosci 32, 4495–4507. https://doi.org/10.1523/JNEUROSCI.3662-11.2012.

Zalesky, A., Fornito, A., Bullmore, E.T., 2010. Network-based statistic: identifying differences in brain networks. Neuroimage 53, 1197–1207. https://doi.org/10.1016/j.neuroimage.2010.06.041.

Zhang, X., Huang, P., Zhang, R., 2022a. Evaluation and Prediction of Post-stroke Cerebral Edema Based on Neuroimaging. Front. Neurol. 12 https://doi.org/10.3389/fneur.2021.763018.

Zhang, Y., Lin, L., Feng, M., Dong, L., Qin, Y., Su, H., Zhou, Z., Dai, H., Wang, Y., 2022b. The mean diffusivity of forceps minor is useful to distinguish amnestic mild cognitive impairment from mild cognitive impairment caused by cerebral small vessel disease. Frontiers in Human Neuroscience 16.